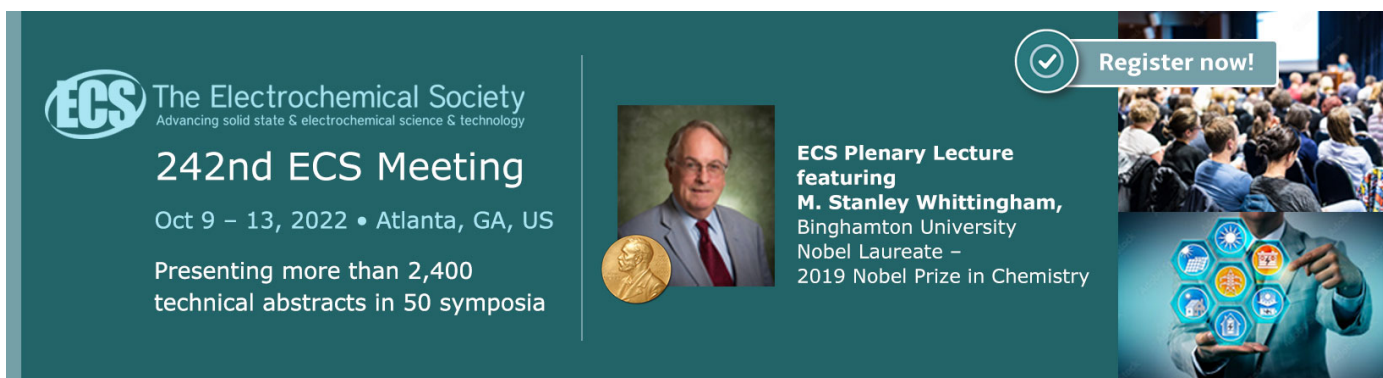


OPEN ACCESS

Assessment of a Modified Hydrocyclone with Ultrasonic Assistance for Nickel Powder Electrochemical Production

To cite this article: Omar González Pérez and José M. Bisang 2022 *ECS Adv.* 1 032501

View the [article online](#) for updates and enhancements.




 The Electrochemical Society
Advancing solid state & electrochemical science & technology

242nd ECS Meeting
Oct 9 – 13, 2022 • Atlanta, GA, US
Presenting more than 2,400
technical abstracts in 50 symposia


ECS Plenary Lecture
featuring
M. Stanley Whittingham,
Binghamton University
Nobel Laureate –
2019 Nobel Prize in Chemistry

 **Register now!**



Assessment of a Modified Hydrocyclone with Ultrasonic Assistance for Nickel Powder Electrochemical Production

Omar González Pérez^z  and José M. Bisang 

Universidad Nacional del Litoral, CONICET, Programa de Electroquímica Aplicada e Ingeniería Electroquímica (PRELINE), Facultad de Ingeniería Química, Santiago del Estero 2829, S3000AOM Santa Fe, Argentina

An electrochemical reactor based on a modified hydrocyclone with ultrasonic assistance is examined with the purpose of analyzing the continuous production of nickel powder from dilute solutions simulating industrial wastewaters containing nickel. Under operating conditions, nickel deposition takes place under mass-transfer control and the helical flow inside the reactor generates a high mass-transfer coefficient, thus improving the removal of metal ions. The application of ultrasound is crucial for the detachment of the electrodeposited nickel, which allows its recovery as a metal powder. The best result was achieved at a current density of 5368 A m^{-2} and $60 \text{ }^\circ\text{C}$ yielding a nickel powder fraction obtained from the spigot of the device higher than 90%. The gravimetric current efficiency and the specific energy consumption were 33.4% and $23.8 \text{ kW h kg}^{-1}$, respectively, for an experiment lasting 13 min. The nickel particles are of high purity and dendritic nature with an average size of $22.9 \text{ }\mu\text{m}$.

© 2022 The Author(s). Published on behalf of The Electrochemical Society by IOP Publishing Limited. This is an open access article distributed under the terms of the Creative Commons Attribution 4.0 License (CC BY, <http://creativecommons.org/licenses/by/4.0/>), which permits unrestricted reuse of the work in any medium, provided the original work is properly cited. [DOI: 10.1149/2754-2734/ac914e]



Manuscript submitted April 27, 2022; revised manuscript received August 22, 2022. Published September 23, 2022.

List of Symbols

a_e	ratio between the electrode surface area and the electrolyte volume, m^{-1}
c	nickel concentration, g dm^{-3} or mol dm^{-3}
d_e	annulus equivalent diameter (difference between the outer and inner diameters in the cylindrical part), m
D	diffusion coefficient, $\text{m}^2 \text{ s}^{-1}$
Da	Damköhler number = k_f/k_m
E_{SCE}	electrode potential referred to saturated calomel electrode, V
F	Faraday constant, $96485.33 \text{ C mol}^{-1}$
gap	inter-electrode gap, m
I	total current, A
j	current density, mA cm^{-2} or A m^{-2}
k	kinetic constant, m s^{-1}
k_f	electrochemical rate constant, m s^{-1}
k_m	mass-transfer coefficient, m s^{-1}
M	nickel molar mass, $58.6934 \text{ g mol}^{-1}$
m	total powder mass, g
m_s	nickel powder mass collected from the spigot, g
n	number of transferred electrons per mole of reactant
q	volumetric flow rate, $\text{dm}^3 \text{ min}^{-1}$
R	nickel fraction obtained from the spigot, %
Re	Reynolds number = $u_{\text{av}} d_e / \nu$
Sc	Schmidt number = ν / D
SCE	saturated calomel electrode
SE	supporting electrode
Sh	Sherwood number = $k_m d_e / D$
SS	stainless steel
t	time, min or h
T	temperature, $^\circ\text{C}$
U	cell potential difference, V
u_{av}	average fluid velocity, m s^{-1}
US	ultrasound
V	total solution volume, dm^3
w^e	specific energy consumption, kW h kg^{-1}
WE	working electrode
x	conversion, %

Greek characters

Φ_C^e	concentration current efficiency, %
Φ_G^e	gravimetric current efficiency, %
σ	space-time yield, $\text{kg m}^{-3} \text{ h}^{-1}$
ν	kinematic viscosity, $\text{m}^2 \text{ s}^{-1}$

Nickel is considered a strategic metal and its global demand is expected to increase in the near future. The primary sources of nickel are mainly in the form of sulfide and laterite ores while the principal secondary resources are nickel-bearing waste including alloys, residues produced in the stainless steel production, spent catalyst, and depleted batteries.¹ In general, aqueous solutions from the leaching of spent batteries are characterized by high nickel concentrations, in the range of 13.5 to 49.5 g dm^{-3} .^{2,3} Moreover, the electrolytes obtained from the dissolution of exhausted catalysts present lower Ni(II) contents, typically between 0.11 and 15 g dm^{-3} .^{4,5} In both cases, pH values are lower than 4 and the electrolytes contain sulfate salts.

Another secondary source of nickel is liquid effluents from commercial processes. Thus, after removal of impurities and pH adjustment, nickel can be recovered starting from the following low-grade raw materials: “acid-killed” laterite leach liquors,⁶ solutions from industrial Watts baths,⁷ copper electrorefining bleed-off electrolytes,⁸ industrial hydrogenated vegetable oil waste,⁹ stainless steel pickling liquors,^{10,11} and spent electroless nickel bath solutions.¹² These electrolytes are characterized by a low Ni(II) concentration, generally in the range of 0.2 to 5 g dm^{-3} .

Accessible and recent techniques for removal of nickel from industrial wastewaters comprise chemical precipitation, ion flotation, ion exchange, membrane filtration, adsorption, photocatalysis, electrochemical methods (electrocoagulation, electrodialysis, electro-deionization, electroflotation, electrochemical reduction), and biological remediation.¹³ However, many of these processes have the following disadvantages: (i) generation of a large amount of sludge, (ii) transfer of Ni(II) ions to another phase that must be further treated by a complementary method, (iii) high associated costs, and (iv) acceptable performances only for low nickel concentrations in solution. Thus, nickel production by electrochemical technologies arises as an attractive option to be explored through the use of continuous flow reactors. Electrowinning of nickel is usually carried out in conventional parallel-plate electrochemical reactors. However, the processing of dilute solutions was also studied with the use of special reactors such as (i) a flow-through porous electrode,¹⁴ (ii) a fluidized bed system,⁶ and (iii) a spouted bed electrochemical reactor.¹⁵

^zE-mail: oglezp@fiq.unl.edu.ar

Table I. Literature review on the electrochemical production of nickel metal powders.

Reactor configuration	Electrolyte (g dm ⁻³)	<i>c</i> (0) (g dm ⁻³)	<i>j</i> (A m ⁻²)	Φ ^e (%)	<i>w</i> ^e (kW h kg ⁻¹)	<i>T</i> (°C)	Remarks	References
Rectangular; Ni cathode and electrolytic Ni anodes	NH ₄ Cl, 300; NaOH, 2	0	215	56	2.3	starting at 24	Gap = 3.8 cm; <i>t</i> = 7 h; Powder purity = 97.5%	21
Rectangular; SS cathode; Ni and graphite anodes	NH ₄ Cl, 54; NaCl, 58; pH 2–3	7	3050	57 ^{a)}	11.4	Up to 50	Gap = 10.2–12.7 cm; <i>V</i> = 19 dm ³ ; <i>t</i> = 1 h; deposit stripped every 15 min; 10 μm particle size; HCl addition	22
Rectangular; refined Ni cathode and anode	NH ₄ OH, 22; pH 12.6	<0.4	90	2–7 ^{a)}	—	Up to 40	Gap = 1.3 cm; <i>t</i> = 2–7 h; [NH ₄ NO ₃] _{final} = 0–2 g dm ⁻³ ; NH ₄ OH addition	23
Tubular concentric; Ni wire cathode and 40 mesh Pt gauze anode	NH ₄ OH, 65; pH 11.5–12	2.4	1 × 10 ⁵	7 ^{a)}	—	50–70	Gap = 0.5–1.5 cm; <i>t</i> = 2.5 h; <i>x</i> = 75%; <i>V</i> = 15 dm ³ ; Three-minutes cathode stripping procedure	24
Rectangular, double compartment; Al net cathode and Ti net anode	(NH ₄) ₂ SO ₄ , 15; H ₃ BO ₃ , 10; pH 3.2	1.74	–1.5 V vs SCE	45	—	Room	Gap = 3 cm; <i>t</i> = 1.33 h; <i>V</i> _{catholyte} = <i>V</i> _{anolyte} = 0.2 dm ³ ; <i>x</i> = 95%	25
Cylindrical; SS rod cathode and Pb-6Sb sheet anode	(NH ₄) ₂ SO ₄ , 40; H ₃ BO ₃ , 10; Thiourea, 0.2; pH 3.2	19.4	5000	45	19.1	55	Gap = 5–6 cm; <i>t</i> = 3.97 h; <i>V</i> = 0.8 dm ³ ; <i>x</i> = 99%; NaOH addition; Powder hydrogen annealing, particle size: 38–213 μm	26
Flow-through; SS cathode and Ni anodes	(NH ₄) ₂ SO ₄ , 132; Trilon B, 26.4; pH <11	5.9	1 × 10 ⁴	35	—	45–48	Powder purity = 97.5%; NH ₄ OH addition	19

a) Calculated from literature values. *c*(0): initial Ni²⁺ concentration, Gap: cathode-anode spacing, *j*: current density, SS: stainless steel, *t*: time, *T*: temperature, *V*: volume, *w*^e: specific energy consumption, *x*: conversion, Φ^e: current efficiency.

Nickel powder is widely used as an alloying element in steel and stainless steel industries, as well as in the development of super-alloys. Other utilizations of Ni powder include cemented carbides, electrical contact materials, porous battery electrodes, filtering devices, and roll compacted strips employed for electrical, electronic, and magnetic applications.¹⁶ Commercially, the two main processes for producing nickel powder are the carbonyl technique and the reduction of a Ni salt aqueous solution with hydrogen under pressure, known as the Sherritt method.¹⁷ However, nickel carbonyl process involves significant danger and harmful conditions because of flammability, explosiveness and high toxicity of the materials used. Moreover, the Sherritt process requires the use of autoclaves at high temperature and 30 bar H₂ pressure.¹⁸ In this context, the production of nickel powder using an electrochemical procedure emerges as an interesting alternative that can compete with more conventional technologies because it requires less demanding operating conditions.¹⁹

The generation of nickel in a finely divided form by electrolytic deposition from aqueous solutions was developed more than eighty years ago. Table I shows various works on the electrochemical production of nickel powder. It is noted that powder manufacturing processes generally involve dilute nickel solutions and continuous pH correction; also, they are characterized by low current efficiencies and thus high specific energy consumptions. In some cases, Ni powder fabrication is an undesired side effect; for instance, a fine nickel powder was generated and collected from the oil phase after induced phase separation at 90 °C during the production of thicker deposits through high internal phase emulsion.²⁰ Moreover, Kovalenko and co-workers¹⁹ call for the development of a pilot-scale reactor for continuous electrochemical synthesis before industrial implementation.

Generally, the electrochemical production of metal powders must be carried out at high current densities, which decreases the performance of the reactors, or by using mechanisms that allow the detachment of the particles lightly adhered to the cathode. Hence, the option of ultrasonic assistance during reactor operation arises as an attractive alternative for the continuous recovery of the electrochemically produced metal dendrites. Thus, the present work concerns the study of a modified hydrocyclone with ultrasonic assistance as an electrochemical reactor for the continuous generation of nickel powder by the use of aqueous solutions simulating effluents containing low concentrations of nickel. Likewise, the characterization of both electrochemical reactor and metal powder is made.

Experimental

Fundamental studies.—A rotating disk electrode (RDE), characterized by a well-defined hydrodynamics, was used with the aim of examining the effect of process variables on the nickel deposition. The electrochemical measurements were carried out using a computer-controlled potentiostat/galvanostat in a three-compartment cell equipped with a water jacket connected to a thermostat. The working electrode (WE) was a 316 L stainless steel or a nickel rotating disk of 0.07 cm² area. Before being used for measurements, the cathode surface was polished by using a felt pad and 0.3 μm alumina paste, cleaned with deionized water in a bath sonicator and dried with a wet filter paper at room temperature. The counter electrode was a platinum wire with a surface area of 3.14 cm². The reference electrode, against which all potentials in this paper are quoted, was a saturated calomel electrode (SCE), attached to a Haber-Luggin capillary. Special attention was paid to the construction and location of the capillary to ensure a small ohmic drop in the solution between its tip and WE. Thus, from a visual point of view, the tip was placed very close to the disk electrode surface. Steady-state open circuit potential of WE was measured, then the potential linearly swept up to a value of -1.20 V at a potential scan rate of 100 mV min⁻¹. The scan rate was chosen as a compromise to obtain polarization curves close to steady-state conditions but without a significant change in the electrode surface area due to metal deposition. All current densities (j) in this work are based on WE geometric area.

The baths consisted of synthetic solutions containing Ni(II) ions and their pH was adjusted either with H₂SO₄ or NH₄OH solutions at room temperature. The supporting electrolyte (SE) contained 36.7 g dm⁻³ (NH₄)₂SO₄ and 30 g dm⁻³ H₃BO₃ at a specified pH. Nickel sulfate hexahydrate, boric acid, ammonium sulfate, sulfuric acid, and ammonium hydroxide were of analytical reagent grade, which were purchased from Cicarelli Laboratories (Santa Fe, Argentina), and used as received. The nickel concentration (c) was spectrophotometrically determined.²⁷ All aqueous solutions were freshly prepared with deionized water (0.4 MΩ cm resistivity).

Nickel powder production with a modified hydrocyclone.—The experimental set-up was a batch recycle system consisting of a hydrocyclone employed as a laboratory-scale reactor, a 5 dm³ reservoir, a pump, a flow meter, valves for control of the volumetric flow rate, and a heat exchanger. Figure 1 depicts the hydrocyclone used in this work and its dimensions, outlined in Table II, were calculated according to the geometric relationships suggested by

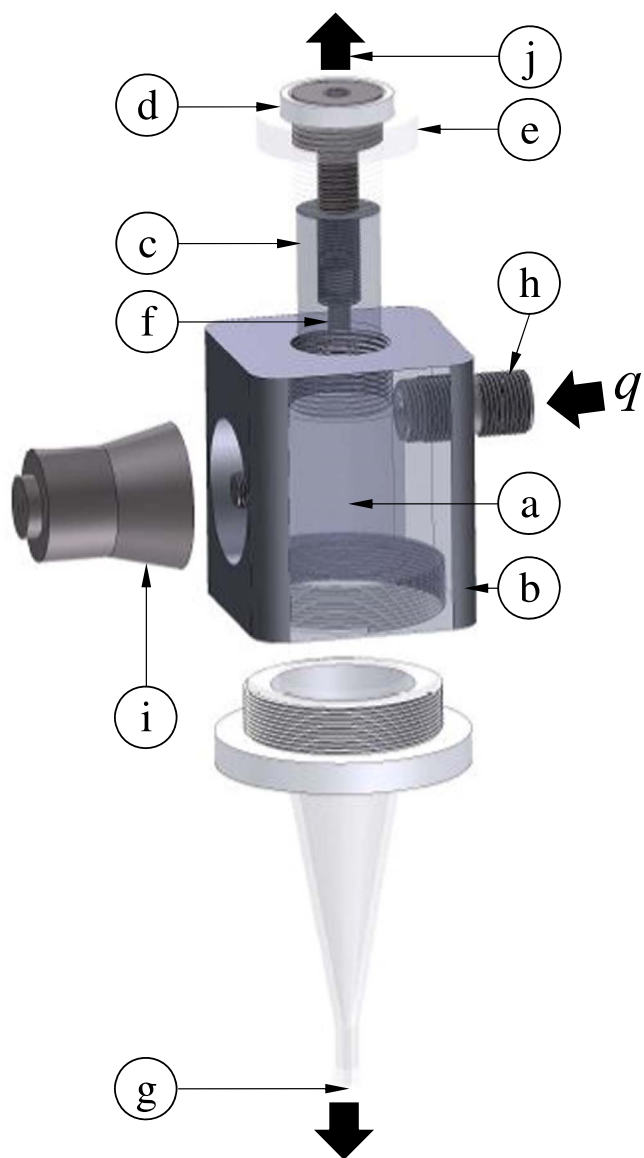


Figure 1. Schematic representation of the modified hydrocyclone reactor with ultrasonic assistance. (a) Cathode; (b) electrical connection to cathode; (c) anode; (d) electrical connection to anode; (e) insulating threaded sleeve; (f) vortex finder; (g) spigot; (h) electrolyte inlet; (i) source of ultrasound; (j) electrolyte overflow. The arrows indicate the flow of the electrolyte. q : inlet liquid volumetric flow rate.

Bradley, providing a standardized device.²⁸ The hydrocyclone was modified to convert it into an electrochemical reactor. Thus, the cylindrical body works as a cathode and it was machined in a 304 stainless steel parallelepiped block, 72 mm side and 85 mm length. The conical part of the hydrocyclone was made of glass. The stainless steel block and the glass cone were assembled together by means of a threaded joint with an O'ring sealing. Cathode surface was polished with 2500 emery paper and copiously washed with deionized water. The anode was a titanium cylinder coated with RuO₂, provided by Laiken S.A. (Buenos Aires, Argentina). The vortex finder was concentric with the anode.

The inter-electrode gap ($0.5d_e$) was 7.3 mm, being d_e the equivalent diameter of the annulus (given by the difference between the outer and inner diameters). The electrolyte was fed into the reactor via a top tangential port. The upper annulus of the cylindrical body at the solution inlet was coated with an epoxy resin or with a Teflon annulus in order to minimize edge effects and prevent the formation of large dendrites that could cause a short circuit during operation. More details about the reactor and the experimental procedure have already been described.²⁹ The total solution volume (V) was 4 dm³ and the reactor volume was 0.0905 dm³.

The stainless-steel block presents a lateral cylindrical housing that allows the horizontal insertion of the ultrasonic horn, which is fastened by means of a threaded screw with plumbing paste in order to ensure a good ultrasound coupling. The source of ultrasound has a power output of 50 W at 40 kHz being 20.9 W the power dissipated in the medium, measured by calorimetry, with an ultrasonic intensity of 1.3 W cm⁻².³⁰

Nickel powder production tests were carried out under galvanostatic conditions. The total current (I), the cell potential difference (U), the solution pH in the storage vessel, and the temperature (T) were monitored. Powders accumulated in the conical part were separated through the spigot at the end of the experiment. These powders and those manually detached from the cathode were washed separately with deionized water and dried in a vacuum stove. Likewise, the same procedure was applied to the small particles of Ni powder accumulated in the reservoir after its separation by filtration. The dimensions and morphology of the nickel powders were characterized using scanning electron microscopy (SEM; Quanta 200 F FEG, FEI, The Netherlands), while their chemical composition was determined by energy dispersive X-ray microanalysis (EDXMA; Genesis, EDAX, USA).

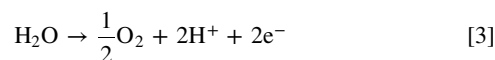
Reactions.—Nickel electrodeposition was the main cathodic reaction, as follows:



and hydrogen evolution occurred as a parasitic reaction



Oxygen evolution was held at the anode



The solution pH in the reservoir during the experiment was kept constant by the addition of an ammonium hydroxide solution to prevent its acidification because of the anodic reaction, Eq. 3.

Definition of the figures of merit.—The total powder mass (m) was determined in order to calculate the gravimetric current efficiency (Φ_G^e), according to

$$\Phi_G^e(t) = \frac{mnF}{MI t} \quad [4]$$

where F is the Faraday constant (96485.33 C mol⁻¹), M is the nickel molar mass (58.6934 g mol⁻¹), n is the number of transferred electrons per mole of reactant (2), and t is the time.

Three-cubic-centimeter samples of the electrolyte were taken from the reservoir at the start and at intervals during the course of the experiment. Taking into account the time variation of nickel concentration, the current efficiency (Φ_C^e) was calculated via

$$\Phi_C^e(t) = \frac{nFV[c(0) - c(t)]}{MI t} \quad [5]$$

Other figures of merit for nickel powder production that characterize the reactor performance were the average values of specific energy consumption (w^e), space-time yield (σ), and conversion (x), which were respectively calculated as follows:

$$w^e = \frac{\int_0^t I(t)U(t)dt}{m} \quad [6]$$

$$\sigma = \frac{m_S}{Vt} \quad [7]$$

$$x = \frac{c(0) - c(t)}{c(0)} 100 \quad [8]$$

Another relevant parameter to be taken into account during the powder generation in a hydrocyclone is the nickel fraction obtained from the spigot (R) given by

$$R = \frac{m_S}{m} 100 \quad [9]$$

where m_S is the nickel powder mass collected from the spigot.

Results and Discussion

Experiments with the rotating disk electrode.—Preliminary experiments were done to examine suitable conditions of pH, temperature, nickel bulk concentration, and cathode material for nickel electrodeposition. For this purpose, current-potential curves were obtained based on the working conditions shown in Table III. In general, at the end of the polarization curves for solutions containing Ni(II) ions, a grayish metallic deposit in the form of an adherent film was observed on the working electrode surface.

Effect of pH.—The effect of pH on nickel electrodeposition from a synthetic effluent was investigated under the experimental

Table II. Geometric parameters of the modified hydrocyclone reactor with ultrasonic assistance.

Parameter	Value (mm)
<i>Cathode section</i>	
Inner cylinder diameter	40
Inner cylinder length	50
Largest cone diameter	40
Smallest cone diameter	2.5
Cone length	113
Cone angle	18°
Spigot opening diameter	2.5
Anode section external diameter	25.4
Length	45
Vortex finder diameter	7
Inlet port diameter	7
Ultrasonic horn diameter	45
Nearest distance of ultrasonic horn to the cathode surface	4

Table III. Standard conditions of the current-potential curves.

Parameter	Value
<i>Bath composition</i>	
Ammonium sulfate	36.7 g dm ⁻³
Boric acid	30 g dm ⁻³
Nickel (II)	2 g dm ⁻³
<i>Polarization curve conditions</i>	
Nitrogen bubbling	No
pH of bulk solution at room temperature	5.5
Potential scan rate	100 mV min ⁻¹
Rotation rate	1000 rpm
Temperature	60 °C
Volume of solution	0.1 dm ³
<i>Electrode parameters</i>	
Working electrode	316 L stainless steel
Size	3 mm in diameter

conditions listed in Table III, except that the pH at room temperature varied between 3 and 9. Table IV presents the pH for different solutions containing Ni(II) ions at room temperature and their corresponding values at 60 °C, the latter being slightly lower than the former.

Figure 2 depicts typical steady-state polarization curves obtained with a 316 L SS rotating disk electrode, where gradual changes are observed. The tones of the lines for each of the current-potential relationships correspond to the visually observed colors of the solutions at each pH. The standard electrode potential for nickel ion reduction, Eq. 1, at 60 °C is -0.45 V vs SCE, while for hydrogen evolution, Eq. 2, is -0.22 V. For the given supporting electrolyte composition and 2 g dm⁻³ Ni(II), the reversible potential of the nickel deposition is -0.55 V against SCE. The activity coefficient of Ni(II) in the multicomponent mixture was calculated by using the Pitzer formalism.³¹ Thus, the thermodynamic analysis predicts that nickel deposition takes place simultaneously with hydrogen evolution.

Figure 2 also shows, in accordance with Armstrong et al.,³² that nickel deposition starts at well negative potentials in comparison with its reversible potential and similar kinetic behavior is shown for a pH range between 3 and 5.5. However, at the highest pH value, a low kinetics is observed due to the formation of hydroxo³³ or ammine complexes^{17,34} of nickel having a smaller diffusion coefficient than the hydrated nickel cations. Thus, the polarization curves of Fig. 2 are not conclusive to define optimal pH values for the experiments. Moreover, a characteristic aspect of nickel deposition is its high sensitivity to the bulk solution pH.³⁵ At pH lower than 3.5 hydrogen evolution becomes intense, resulting in a decrease in current efficiency and hydrogenation of the deposit. Therefore, to minimize hydrogen evolution, it is necessary to operate at a pH around neutrality.²⁹ On the contrary, at pH higher than 5.6 the basic salts of nickel precipitate near the cathode and are incorporated into the growing deposit. Likewise, taking into consideration the thermodynamic data of the Ni(II)-H₂O system³¹ and in order to avoid the precipitation of Ni(OH)₂, the pH for aqueous solutions without buffers must remain below 6 for a 2 g dm⁻³ Ni(II) solution. The use of a solution containing boric acid and ammonium sulfate prevents the precipitation of nickel hydroxide, increasing the pH value at which nickel deposition can take place.

Also, it was reported that the maximum nickel recovery from some polluting effluents was obtained within a pH interval of 4.66–5.55 at temperatures higher than 50 °C.^{26,36} In addition, Njau and Janssen³⁷ report that the current efficiency goes through a maximum at about a pH of 5 when using a solution containing NiSO₄ and (NH₄)₂SO₄. Based on the above statements, a pH of 5.5 was chosen for the following tests.

Table IV. Effect of temperature and Ni(II) concentration on pH values for selected electrolytes.

Solution	pH at room temperature	pH at 60 °C
SE + c = 2 g dm ⁻³	3.00	2.78
SE + c = 0.2 g dm ⁻³	5.50	5.38
SE + c = 2 g dm ⁻³	5.50	4.86
SE + c = 5 g dm ⁻³	5.50	4.72
SE + c = 2 g dm ⁻³	6.00	5.37
SE + c = 2 g dm ⁻³	7.00	6.41

SE: supporting electrolyte; 36.7 g dm⁻³ (NH₄)₂SO₄ and 30 g dm⁻³ H₃BO₃.

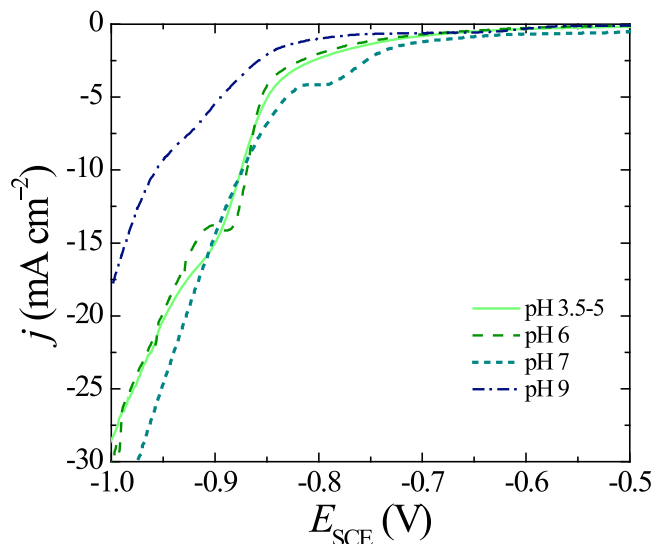


Figure 2. Current-potential curves for the reduction of nickel at a 316 L stainless steel rotating disk electrode at different pH values. $c = 2$ g dm⁻³ Ni(II). Supporting electrolyte: 36.7 g dm⁻³ (NH₄)₂SO₄ and 30 g dm⁻³ H₃BO₃. Potential scan rate: 100 mV min⁻¹. Rotation rate: 1000 rpm. $T = 60$ °C.

Effect of temperature.—Electrolyte temperature was varied between 25 and 70 °C in the tests where the effect of temperature was investigated, while the remaining parameters declared in Table III were maintained. The full lines in Fig. 3 show the polarization curves at different temperatures whereas the dashed and dotted lines correspond to the supporting electrolyte at 25 and 60 °C, respectively. The comparison between the dashed and dotted lines with the corresponding polarization curves for the system confirms that hydrogen evolution and nickel deposition take place simultaneously at the electrode surface over the entire examined potential range. However, the rate of nickel deposition noticeably rises as the temperature increases showing that nickel recovery is convenient at temperatures higher than 50 °C.

Several authors reported that increasing the temperature above room temperature benefits nickel electrodeposition, since it increases the conductivity of the electrolyte, raises the mass and charge transfer of Ni(II) ions and lowers the equilibrium potential of the reaction of interest. Temperatures close to 50 °C are used for this purpose.^{3,6,7,14,36–43} On an industrial scale, Ni electrowinning is performed at 60 °C from purified solutions containing chlorides or sulfates.¹⁸ Likewise, the specific case of electrochemical production of nickel powder is carried out in the temperature range from 45 to 70 °C,^{19,24,26} being the powders obtained at these temperatures very fine and easy to grind. However, excessively high temperatures, above 70 °C, should be avoided because Ni(II) hydroxide precipitation is favored.⁴¹ Therefore, 60 °C was adopted as the working temperature in the present study.

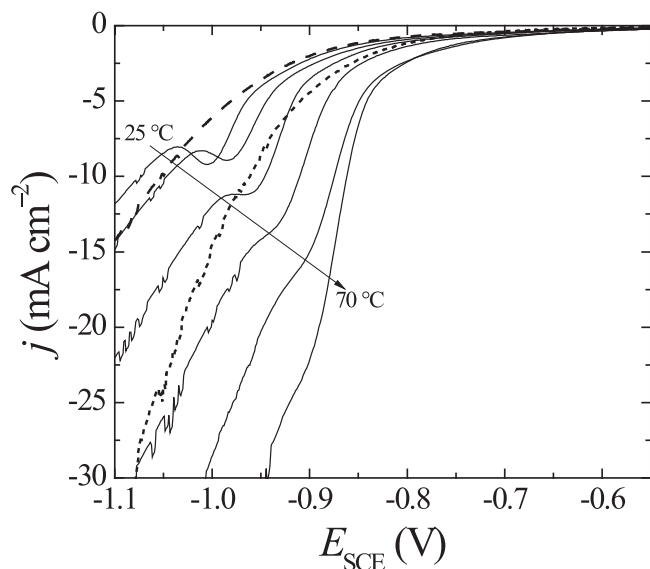


Figure 3. Current-potential curves for the reduction of nickel at a 316 L stainless steel rotating disk electrode for different temperatures. Full lines: Ni (II)-containing solutions at 25, 30, 40, 50, 60, and 70 °C. Dashed line: supporting electrolyte at 25 °C. Dotted line: supporting electrolyte at 60 °C. $c = 2 \text{ g dm}^{-3}$ Ni(II). Supporting electrolyte: 36.7 g dm^{-3} $(\text{NH}_4)_2\text{SO}_4$ and 30 g dm^{-3} H_3BO_3 . pH = 5.5. Potential scan rate: 100 mV min^{-1} . Rotation rate: 1000 rpm.

Effect of nickel concentration.—Trials were carried out using the 316 L stainless steel rotating disk electrode with nickel ion concentration in the range of $0.2\text{--}5 \text{ g dm}^{-3}$ and all other operating conditions declared in Table III being held constant. The results of these experiments are shown in Fig. 4. For the sake of comparison, the polarization curve for the supporting electrolyte is also reported in dashed line. Figure 4 reveals that nickel deposition is possible from dilute solutions and, as expected, for a given value of electrode potential the reaction rate increases as the nickel concentration is raised. Furthermore, 2 g dm^{-3} of nickel in solution is within the typical concentration found in wastewaters used in electrochemical treatment technologies.^{36,44} For this reason, the above value of nickel concentration was applied in the following experiments.

Effect of cathode material.—Figure 5 illustrates the effect of the material (316 L stainless steel and nickel) on nickel deposition according to the experimental conditions described in Table III, including as dashed lines the polarization curves for the supporting electrolyte. It is observed that the electrochemical behavior of nickel deposition reaction is similar for both materials. The inset in Fig. 5 represents the difference in the polarization curves with and without nickel in the solution for each electrode material, corroborating that nickel deposition takes place across the full range of potentials. Figure 5 also demonstrates that 316 L stainless steel represents an appropriate starting material for the cathode and during operation it is covered with nickel. In view of nickel being more expensive than stainless steel, the latter was used as the cathode material in the experiments with the modified hydrocyclone as an electrochemical reactor.

Experiments with a modified hydrocyclone.—All experiments were performed at 60 °C under galvanostatic control until the theoretical electrical charge necessary to deposit the initial nickel, also termed the stoichiometric charge, was passed. The theoretical charge was calculated according to Faraday's law assuming 100% current efficiency, resulting in 26302 C for 4 dm^3 solution with an initial nickel concentration of 2 g dm^{-3} . Thus, Fig. 6 shows the figures of merit as a function of the current density; the upper abscissa axis represents the total current and the upper secondary abscissa axis the duration of the experiment. It can be observed that

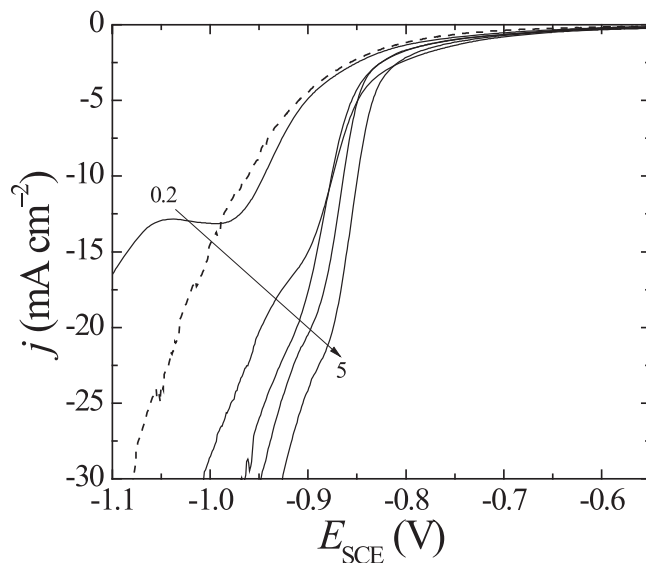


Figure 4. Current-potential curves for the reduction of nickel at a 316 L stainless steel rotating disk electrode. Full lines: Ni(II)-containing solutions at 0.2, 2, 3, 4, and 5 g dm^{-3} . Dashed line: supporting electrolyte. Supporting electrolyte: 36.7 g dm^{-3} $(\text{NH}_4)_2\text{SO}_4$ and 30 g dm^{-3} H_3BO_3 . pH = 5.5. $T = 60 \text{ °C}$. Potential scan rate: 100 mV min^{-1} . Rotation rate: 1000 rpm.

both the current efficiency and the nickel conversion decrease when the current density is increased due to the secondary cathodic reaction of hydrogen evolution becomes more significant. Also, as expected, both the cell potential difference and the specific energy consumption increase.

Considering the nickel fraction obtained from the spigot as the most important parameter to characterize the process, the best result was obtained at a current density of 5368 A m^{-2} , giving a maximum value of R higher than 90%, being the figures of merit summarized in the first row in Table V. The second row in Table V shows the results from an experiment with 50 min duration, where a higher conversion (70.9%) was achieved. A comparison of the first two rows in Table V allows us to observe that the electrochemical parameters that characterize the reactor worsen when the electrolysis time increases because, under galvanostatic operation, the decrease in nickel concentration favors hydrogen evolution as the predominant cathodic reaction. However, the value of R is high, allowing the deposited nickel to be removed from the spigot as a metal powder. The third row in Table V reports the figures of merit for an experiment at the same current density but under silent conditions showing that the electrodeposited nickel remains attached to the cathode surface and only 1.7% was obtained as a powder from the spigot. The eighth column in Table V lists the space-time yields, referred to Ni mass obtained from the spigot, in order to characterize the performance of the reactor for the continuous production of metal powder, showing that high σ values are achieved under ultrasonic operation. The other figures of merit in the first and third rows in Table V show similar values under both working conditions. Therefore, the detachment of electrodeposited nickel is mainly a consequence of the application of ultrasound to the modified hydrocyclone. The impingement effect of the helical flow on the cathode and the intense hydrogen evolution have a marginal influence on its detachment. Moreover, the second and third columns in Table V show that the gravimetric and concentration current efficiencies are quite similar in all trials.

Figure 7 displays the temporal variation of the dimensionless concentration in the reservoir for the experiments reported in Fig. 6. As expected, the concentration diminishes with time and the decay is more marked when the current density increases.

The change in concentration with time for a recirculating electrochemical system, assuming a first-order kinetics at high

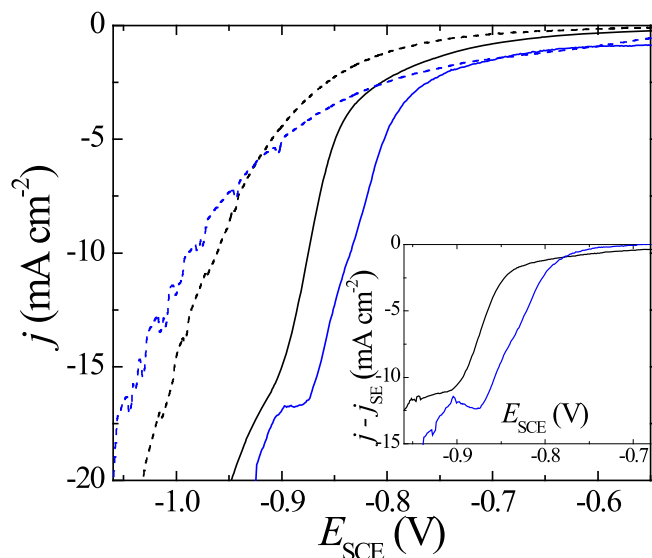


Figure 5. Current-potential curves for the reduction of nickel at a rotating disk electrode. Full black line: 316 L stainless steel. Dashed black line: supporting electrolyte, 316 L stainless steel. Full blue line: nickel. Dashed blue line: supporting electrolyte, nickel. $c = 2 \text{ g dm}^{-3}$ Ni(II). Supporting electrolyte: 36.7 g dm^{-3} $(\text{NH}_4)_2\text{SO}_4$ and 30 g dm^{-3} H_3BO_3 . pH = 5.5. $T = 60 \text{ }^\circ\text{C}$. Potential scan rate: 100 mV min^{-1} . Rotation rate: 1000 rpm. Inset: Difference between total current density and current density in the absence of Ni(II) ions (SE).

overpotentials and that the reservoir is a well-mixed tank, is given by the following relationship:⁴⁵

$$c(t) = c(0)e^{-ka_e t} \quad [10]$$

which is valid when the reactor volume is negligible compared to the reservoir volume. In the last equation, a_e is the ratio between the electrode surface area and the electrolyte volume. The kinetic constant (k) is provided by

$$k = k_m \frac{\text{Da}}{1 + \text{Da}} \quad [11]$$

where the Damköhler number (Da) is defined as the ratio of the electrochemical rate constant (k_f) to the mass-transfer coefficient (k_m).⁴⁶ For Da much higher than one, k approaches k_m and Eq. 10 gives the change of concentration in the electrochemical system for a reaction under mass-transfer control in accordance with

$$c(t) = c(0)e^{-k_m a_e t} \quad [12]$$

The mass-transfer coefficient for the cylindrical part of the hydrocyclone can be evaluated from the following dimensionless relationship between the Sherwood (Sh), Reynolds (Re), and Schmidt (Sc) numbers:⁴⁷

$$\text{Sh} = 0.513 \text{Re}^{0.79} \text{Sc}^{1/3} \quad [13]$$

The physicochemical parameters for the evaluation of the dimensionless numbers were calculated as follows. The diffusion coefficient (D) of nickel ion at $25 \text{ }^\circ\text{C}$ was reported by Sanborn and Orlemann⁴⁸ as $5.6 \times 10^{-10} \text{ m}^2 \text{ s}^{-1}$, which was corrected by

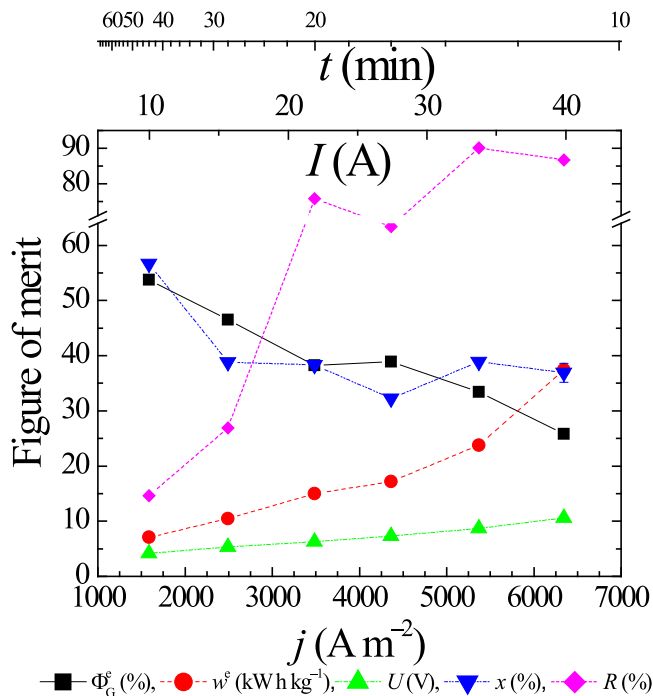


Figure 6. Figures of merit as a function of the total current density for the modified hydrocyclone. $c(0) \sim 2 \text{ g dm}^{-3}$ Ni(II). Supporting electrolyte: 36.7 g dm^{-3} $(\text{NH}_4)_2\text{SO}_4$ and 30 g dm^{-3} H_3BO_3 . pH = 5.5. $T = 60 \text{ }^\circ\text{C}$. Total charge in each experiment: 26302 C. $q = 9.6 \text{ dm}^3 \text{ min}^{-1}$.

temperature according to the Stokes-Einstein relationship giving a value of $1.2 \times 10^{-9} \text{ m}^2 \text{ s}^{-1}$ at $60 \text{ }^\circ\text{C}$. The kinematic viscosity (ν) was assumed to be $5 \times 10^{-7} \text{ m}^2 \text{ s}^{-1}$. Therefore, a theoretical value for $k_m a_e$ of $3 \times 10^{-2} \text{ min}^{-1}$ was calculated at a volumetric flow rate of $9.6 \text{ dm}^3 \text{ min}^{-1}$ and $60 \text{ }^\circ\text{C}$. The full line in Fig. 7 stands for Eq. 12 with the above $k_m a_e$ value. Figure 7 also shows that the concentration change is lower than that predicted by Eq. 12 for the lowest total current densities, indicating that nickel deposition is under combined activation and mass transport control. However, as the total current density increases the experimental data agree quite well with Eq. 12 and also with results without sonication, within the accuracy expected for experiments involving metal deposition, showing a mass-transfer control for nickel deposition. Therefore, the helical flow defines the high mass-transfer coefficient in the modified hydrocyclone and the effect of both hydrogen evolution and sonication are irrelevant to this parameter. It must be remarked that nickel deposition changes the electrode surface area increasing its roughness which in turn enhances k_m and modifies a_e . The effect of the surface roughness was neglected in the theoretical treatment because it takes place in an unpredictable manner. However, the consideration of the increase in $k_m a_e$ due to the electrode roughness generates a decay in concentration greater than that shown as full line in Fig. 7. Thus, the dependence of the kinetic control type on the current density, stated above, remains valid.

Characterization of the nickel powder.—Figure 8 shows a typical micrograph of a nickel powder sample obtained from the spigot for the experiment stated in the first row in Table V. It can be observed that the particles are predominantly globules with a

Table V. Comparison of the figures of merit under ultrasonic and silent conditions at $j = 5368 \text{ A m}^{-2}$ (maximum value of R in Fig. 6).

Operation	Φ_G^e (%)	Φ_C^e (%)	w^e (kW h kg ⁻¹)	U (V)	x (%)	R (%)	σ (kg m ⁻³ h ⁻¹)	t (min)
Sonic	33.4	32.8	23.8	8.7	38.9	90.1	122.9	13
Sonic	21.3	18.0	36.8	8.6	70.9	56.3	49.0	50
Silent	33.7	32.3	21.7	8.0	31.3	1.7	2.3	13

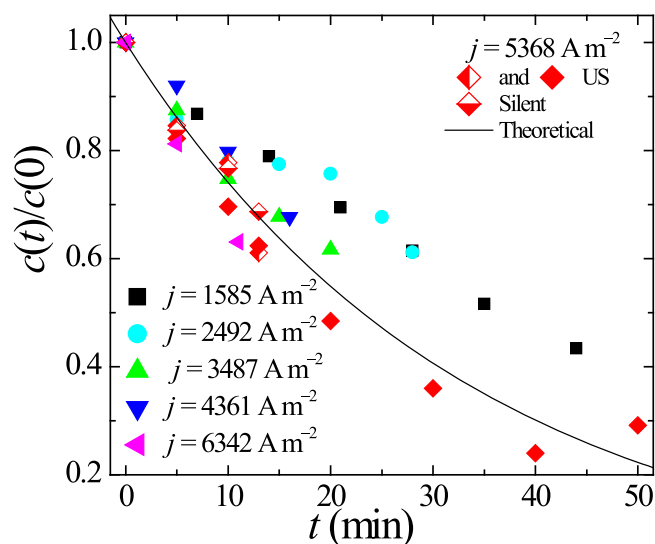


Figure 7. Concentration in the reservoir as a function of time. $c(t) \sim 2 \text{ g dm}^{-3} \text{ Ni(II)}$. Supporting electrolyte: $36.7 \text{ g dm}^{-3} (\text{NH}_4)_2\text{SO}_4$ and $30 \text{ g dm}^{-3} \text{ H}_3\text{BO}_3$. pH = 5.5. $T = 60 \text{ }^\circ\text{C}$. $q = 9.6 \text{ dm}^3 \text{ min}^{-1}$. Full line: theoretical prediction under limiting current conditions, Eq. 12.

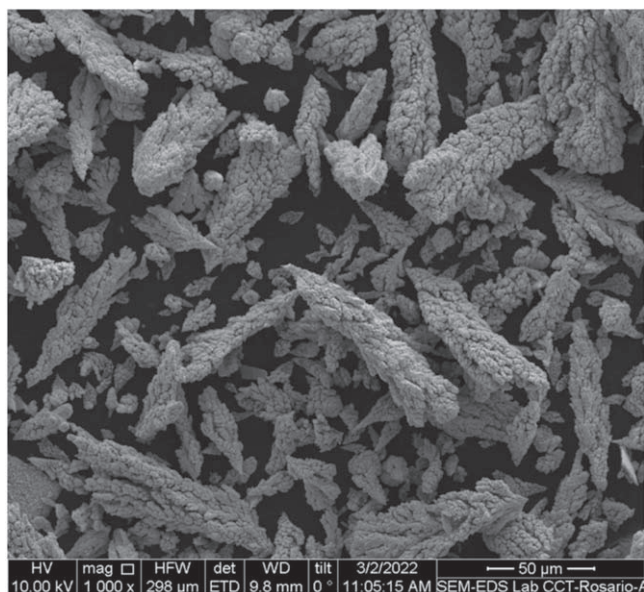


Figure 8. Scanning electron micrograph of nickel powder obtained from the spigot. Magnification: $\times 1000$. $j = 5368 \text{ A m}^{-2}$. $I = 33.7 \text{ A}$. $T = 60 \text{ }^\circ\text{C}$. $t = 13 \text{ min}$ $q = 9.6 \text{ dm}^3 \text{ min}^{-1}$.

dendritic nature having different sizes as it is reported in the histogram of Fig. 9. The largest dimension of the particles was used for the statistical analysis based on 974 independent size measurements, being the average value of the particles $22.9 \mu\text{m}$ with a standard deviation of $19.3 \mu\text{m}$. It must be remarked that the particle size is considerably lower than that previously reported,²⁶ declared in Table I, and the powder is within the convenient size range, from 5 to $50 \mu\text{m}$, stated by Kovalenko et al.¹⁹ for the manufacture of superalloys. The EDS study of the nickel powders showed an average composition value of 98.7 wt% Ni and 1.3 wt% oxygen. No other elements that may come from the materials used in the electrodes were detected, which corroborates their stability under operating conditions. For applications requiring a lower oxygen fraction, it is necessary to subject the powder to annealing in a furnace at a high temperature with a flow of hydrogen gas.²⁶

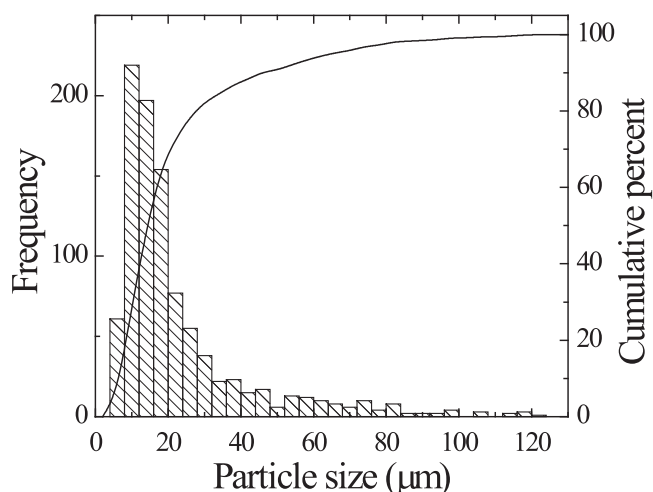


Figure 9. Distribution of particle size of nickel powder obtained from the spigot. $j = 5368 \text{ A m}^{-2}$. $I = 33.7 \text{ A}$. $T = 60 \text{ }^\circ\text{C}$. $t = 13 \text{ min}$ $q = 9.6 \text{ dm}^3 \text{ min}^{-1}$.

Conclusions

From the above paragraphs the following conclusions can be drawn:

- The ultrasonic assistance plays an essential role in the detachment of the metal deposit allowing its recovery as a nickel powder from the spigot of the hydrocyclone. The impingement effect of the helical flow on the cathode surface and the hydrogen evolution are irrelevant for this purpose.
- The high value of the mass-transfer coefficient for nickel deposition is a consequence of the intense convection produced by the helical flow in the cylindrical part of the hydrocyclone and also of the increase in the electrode roughness. The application of ultrasound and hydrogen evolution has little influence on the mass-transfer conditions.
- The use of titanium coated with RuO_2 as an anode is essential to obtain a powder of high purity, which represents an important advance compared to previous studies.
- A modified hydrocyclone with ultrasonic assistance is a promising electrochemical reactor because it presents a high space-time yield and allows the continuous production of nickel powder with high purity.
- The continuous electrochemical production constitutes a considerable improvement for the current practice of nickel powder manufacture.

Acknowledgments

This work was supported by the Agencia Nacional de Promoción Científica y Tecnológica (ANPCyT), Consejo Nacional de Investigaciones Científicas y Técnicas (CONICET) and Universidad Nacional del Litoral (UNL) of Argentina. The authors would like to thank Laiken S.A. (Argentina) for supplying the anode material.

ORCID

Omar González Pérez  <https://orcid.org/0000-0003-3482-5409>
José M. Bisang  <https://orcid.org/0000-0001-9120-7418>

References

1. G. Alvia-Hein, H. Mahandra, and A. Ghahreman, *J. Clean. Prod.*, **297**, 126592 (2021).
2. C. Hazotte, N. Leclerc, E. Meux, and F. Lapique, *Hydrometall.*, **162**, 94 (2016).
3. C. Lupi, M. Pasquali, and A. Dell'Éra, *Waste Manage.*, **25**, 215 (2005).
4. W. Mulak, B. Miazga, and A. Szymczycha, *Int. J. Miner. Process.*, **77**, 231 (2005).
5. K. K. Sahu, A. Agarwal, and B. D. Pandey, *Waste Manage. Res.*, **23**, 148 (2005).

6. W. G. Sherwood, P. B. Queneau, C. Nikolic, and D. R. Hodges, *Metall. Trans. B*, **10**, 659 (1979).
7. E. Avci, *Sep. Sci. Technol.*, **24**, 317 (1989).
8. R. L. Nyirenda and W. S. Phiri, *Miner. Eng.*, **11**, 23 (1998).
9. Sirajuddin, L. Kakakhel, G. Lutfullah, and R. U. Marwat, *Acta Chim. Slov.*, **51**, 793 (2004).
10. J. Hermoso, J. Dufour, J. L. Gálvez, C. Negro, and F. López-Mateos, *Ind. Eng. Chem. Res.*, **44**, 5750 (2005).
11. F. Rögener, M. Sartor, A. Bán, D. Buchloh, and T. Reichardt, *Resour. Conserv. Recycl.*, **60**, 72 (2012).
12. R. Idhayachander and K. Palanivelu, *E-J. Chem.*, **7**, 1412 (2010).
13. V. Kumar and S. K. Dwivedi, *J. Clean. Prod.*, **295**, 126229 (2021).
14. P. Singh and M. Totlani, *J. Electrochem. Soc. India*, **28**, 143 (1979).
15. P. Grimshaw, J. M. Calo, P. A. Shirvanian, and G. Hradil, *Ind. Eng. Chem. Res.*, **50**, 9525 (2011).
16. J. R. Davis, *ASM Specialty Handbook: Nickel, Cobalt, and Their Alloys*, ed. J. R. Davis (ASM International, Ohio, USA) p. 10 (2000).
17. S. S. Naboychenko, I. B. Murashova, and O. D. Neikov, *Handbook of Non-Ferrous Metal Powders: Technologies and Applications*, ed. O. D. Neikov et al. (Amsterdam)(Elsevier, Oxford, UK) p. 369 (2009).
18. F. K. Crundwell, M. S. Moats, V. Ramachandran, T. G. Robinson, and W. G. Davenport, *Extractive Metallurgy of Nickel, Cobalt and Platinum-Group Metals* (Elsevier, Oxford, UK) p. 347 (2011).
19. V. Kovalenko, V. Kotok, and S. Vlasov, *East-Eur. J. Enterp. Technol.*, **1**, 27 (2018).
20. I. J. Brown and S. Sotiropoulos, *Electrochim. Acta*, **46**, 2711 (2001).
21. C. L. Mantell, *US Patent*, 2233103A (1941).
22. S. A. Mayper, *US Patent*, 2625507 (1953).
23. L. J. Wrangell, *US Patent*, 3458407A (1969).
24. J. P. Murdock, W. Allis, and D. Pouli, *US Patent*, 3510408A (1970).
25. C. Lupi and M. Pasquali, *Miner. Eng.*, **16**, 537 (2003).
26. A. Agrawal, D. Bagchi, S. Kumari, V. Kumar, and B. D. Pandey, *Powder Technol.*, **177**, 133 (2007).
27. J. P. Mehlis, *Ind. Eng. Chem. Anal. Ed.*, **14**, 289 (1942).
28. D. Bradley, *The Hydrocyclone* (Pergamon, Oxford, UK) (1965).
29. O. González Pérez and J. M. Bisang, *Chem. Eng. Process.*, **168**, 108560 (2021).
30. J. P. Fornés and J. M. Bisang, *Electrochim. Acta*, **213**, 186 (2016).
31. K. S. Pitzer, *Activity Coefficients in Electrolyte Solutions* (CRC Press, Boca Raton, USA) 2nd. ed. (2018).
32. R. D. Armstrong, M. Todd, J. W. Atkinson, and K. Scott, *J. Appl. Electrochem.*, **26**, 379 (1996).
33. E. Vallés, R. Pollina, and E. Gómez, *J. Appl. Electrochem.*, **23**, 508 (1993).
34. I. Rodríguez-Torres, G. Valentin, and F. Lapicque, *J. Appl. Electrochem.*, **29**, 1035 (1999).
35. Y. D. Gamburg and G. Zangari, *Theory and Practice of Metal Electrodeposition* (Springer, New York, USA) (2011).
36. G. Orhan, C. Arslan, H. Bombach, and M. Stelter, *Hydrometall.*, **65**, 1 (2002).
37. K. N. Njau and L. J. J. Janssen, *J. Appl. Electrochem.*, **25**, 982 (1995).
38. B. D. Barker and B. A. Plunkett, *Trans. IMF*, **54**, 104 (1976).
39. V. Kumar, B. D. Pandey, and D. D. Akerkar, *Hydrometall.*, **24**, 189 (1990).
40. B. D. Pandey and V. Kumar, *Hydrometall.*, **26**, 35 (1991).
41. J. Ji, W. C. Cooper, D. B. Dreisinger, and E. Peters, *J. Appl. Electrochem.*, **25**, 642 (1995).
42. D. A. Bertuol, F. D. R. Amado, H. Veit, J. Z. Ferreira, and A. M. Bernardes, *Chem. Eng. Technol.*, **35**, 2084 (2012).
43. S. Awasthi, S. Goel, C. P. Pandey, and K. Balani, *JOM*, **69**, 227 (2017).
44. K. N. Njau, M. v Woude, G. J. Visser, and L. J. J. Janssen, *Chem. Eng. J.*, **79**, 187 (2000).
45. A. N. Colli and J. M. Bisang, *Electrochim. Acta*, **58**, 406 (2011).
46. K. Scott, *Electrochemical Reaction Engineering* (Academic Press Inc, London, UK) (1991).
47. L. C. Resio, O. González Pérez, and J. M. Bisang, *J. Electrochem. Soc.*, **164**, E529 (2017).
48. R. H. Sanborn and E. F. Orlemann, *J. Am. Chem. Soc.*, **77**, 3726 (1955).